Results from helical axis stellarators

B. D. Blackwell

Citation: Physics of Plasmas (1994-present) **8**, 2238 (2001); doi: 10.1063/1.1364671
View online: http://dx.doi.org/10.1063/1.1364671
View Table of Contents: http://scitation.aip.org/content/aip/journal/pop/8/5?ver=pdfcov
Published by the AIP Publishing

Results from helical axis stellarators*

B. D. Blackwell†
Plasma Research Laboratory, Research School of Physical Sciences and Engineering, Australian National University, Canberra 0200, Australia

(Received 27 October 2000; accepted 22 February 2001)

Helical axis stellarators produce magnetic surfaces of high rotational transform and moderate shear solely by means of external currents, with the promise of high β. Several machines with quite different toroidal, helical, and ''bumpy'' Fourier components of magnetic field are now producing results, including high quality magnetic surfaces, confinement mode transitions, configuration studies, and confinement consistent with International Stellarator Scaling (ISS95) scaling up to $T_e \sim 2$ keV. These devices permit concept evaluation over an unprecedented configuration space, and allow basic comparisons with those designed by established and alternative optimization strategies. © *2001 American Institute of Physics.* [DOI: 10.1063/1.1364671]

I. INTRODUCTION

The *stellarator*[1] is a magnetic configuration in which the magnetic field lines form and cover a set of nested *magnetic surfaces* which confine plasma solely by means of external currents. Helical axis stellarators are a class of *spatial axis*[2] stellarators, in which the magnetic axis *(the limiting magnetic surface of zero enclosed volume)* traces a path which deviates from the usual straight line or circle, in a helical manner. This modifies the curvature of the magnetic field lines on all surfaces, most notably by generating *rotational transform* (ι: poloidal twist per toroidal turn) resulting from axis torsion: formally, the integral of the torsion around the magnetic axis [Fig. 1(a)]. The first stellarator, conceived by Spitzer[1] in 1951, had a spatial axis in the shape of a figure-8 twisted out of the plane [Fig. 1(b)] so that the return legs did not intersect. This generated a rotational transform of ~ 0.1. The helical spatial axis, which has a more uniform distribution of torsion, was proposed by Koenig[3] in connection with the use of low order helical windings, now referred to as $l=1$ windings,[1] but as is explained in the following, Spitzer's early machines employed higher order windings.

It was known that toroidal devices tend to form a magnetic *hill* in which the magnetic field decreases in directions away from the axis [in an average sense: see the discussion of Eq. (1)], and that this made the plasma unstable to the magnetohydrodynamic (MHD) interchange mode.[4] Spitzer proposed shear (transform increasing with radius) stabilization of this mode, which was later demonstrated theoretically for a stellarator under the assumptions of ideal (plasma resistivity $\rightarrow 0$) MHD.[4] This was provided by higher order helical windings ($l=2,3$).

Experimental results were initially discouraging, but it was not clear at the time to what extent this was due to technological problems such as impurities, and the need to produce and heat the confined plasma with internal currents which significantly affected the magnetic configuration. Doubt was cast on the applicability of ideal MHD theory in that although the resistivity was indeed very small, and could be expected to decrease with the attainment of higher temperatures, small scale-length instabilities could develop for which the resistivity could not be ignored,[5] leading to a ''resistive interchange'' instability. This motivated a renewed interest in stabilization by magnetic well, which gave rise to the discovery of several interesting configurations with this property, including the helical axis configuration (now known as the heliac)[6] in the ''straight'' or pure helical limit, and some that were toroidal. The magnetic well was achieved in the average sense in that the quantity

$$V' \equiv 1/N \int dl/B \tag{1}$$

was maximum on axis, or more precisely when the derivative of (1) is of the opposite sign to the pressure gradient; i.e., V'' is negative. Here V is the volume enclosed by the magnetic surface, the prime($'$) denotes the derivative with

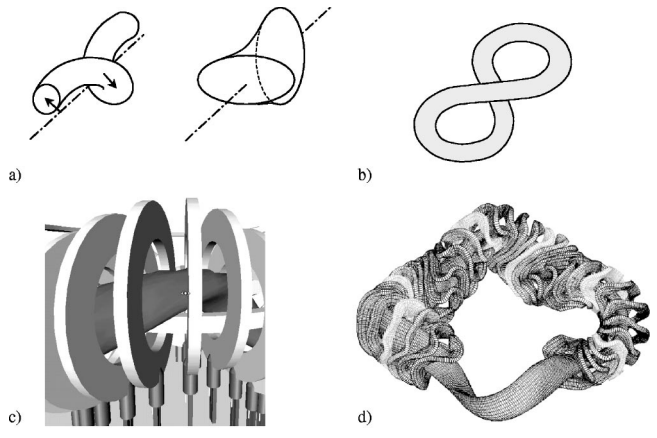

FIG. 1. (a) Two geometric methods of transform generation: axis torsion due to a helical axis, and rotation of elliptical surface cross sections. (b) Figure-8 configuration. (c) Partial side view of the heliac coil configuration showing the planar TF coils, and the bean-shaped plasma encircling the central ring. (d) HSX configuration showing 36 of the 48 non-planar coils and the last closed flux surface of the plasma.

*Paper UI1 3, Bull. Am. Phys. Soc. **45**, 289 (2000).
†Invited speaker.

respect to the enclosed magnetic flux, and V', the specific volume[7] [which may be evaluated by (1), integrating along the magnetic field line (dl) over N toroidal circuits for a rational surface, or taken to the limit of large N otherwise]. Physically the interchange of inner and outer plasma flux tubes is (marginally) stabilized by making the process energy neutral, because for the case of magnetic well, the magnetic and thermal energy densities have opposite radial dependences (and therefore derivatives of opposite sign). One feature common to several of these configurations was the concept (attributed to Yoshikawa[6]) of causing magnetic field lines to ''linger'' in regions of *favorable curvature* (''local'' magnetic well) by the use of a ''stagnation'' winding. Magnetic well is discussed in some detail in relation to magnetic geometry by Furth[8] and recently by Greene.[9] Significantly, minimum B in the average sense admits the possibility, occurring in many configurations with average magnetic well, that *local* magnetic hills exist (regions of bad curvature), leading to localized instabilities such as ballooning modes.

The Asperator NP[10] was an early helical axis device. Like the figure-8 stellarator, this device used a solenoidal toroidal field wound following a noncircular axis which was for the first time a toroidal helix, with a *toroidal periodicity* **N** of 16. Toroidal effects were partly compensated by the use of additional helical windings. A toroidal heliac device (''HX-1'') was proposed in 1982–4,[11–13] realized purely with circular conductors configured as a toroidal solenoid with a helical axis, linked by a central ring conductor [Fig. 1(c)]. The rotational transform from axis torsion was augmented in the heliac by rotation of the plasma cross section [Fig. 1(a)], resulting in a net transform about half the number of rotations ($\iota \sim N/2$). This device was never built; the first heliac plasma was demonstrated in 1984 in SHEILA,[14] a small $N=3$ prototype inspired by that proposal. Larger machines followed: the Tohoku heliac (1987),[15] the **H-1 heliac** (Australian National University, Canberra, 1992),[16] and the **TJ-II flexible heliac** (CIEMAT, Madrid, 1996).[17] A linear heliac/pinch (1987[18]) allowed short pulse experiments at high β, testing (on a very short time scale) the predictions of high β limits for heliacs.[19,20]

Both H-1 and the TJ-II heliacs are ''flexible'' heliacs,[21] which by the addition of a single $l=1$ winding around the ring conductor, became highly flexible in magnetic configuration. Typically ι variation was greater than a factor of 2, and magnetic well control ranged from in excess of 5% well to the extreme of magnetic hills over at least part (outside) of the plasma volume. A new advanced configuration, the **helical-axis heliotron, Heliotron J**[22] (Kyoto University, 1999), the successor to Heliotron E, uses a ''bumpy'' magnetic component to improve high-energy particle confinement and reduce neoclassical transport via quasi-isodynamic optimization. A combination of toroidal and helical coils produces a range of configurations. The **Helically Symmetric Experiment**[23] ''HSX'' [Univ. Wisconsin, Madison, 1999, Fig. 1(d)] employs computer optimized nonplanar coils to exploit (for the first time) a quasisymmetry that minimizes the nonhelically symmetric magnetic field harmonics.

TABLE I. Parameters of the helical axis stellarators discussed.

Device	H-1	TJ-II	Heliotron J	HSX
B_0 (T)	1.0	1.2	1.5	1.25
$R(m)$	1.0	1.5	1.2	1.2
$\langle a \rangle (m)$	0.1–0.2	0.1–0.22	0.1–0.18	0.15
N	3	4	4	4
Aspect ratio	$\geqslant 5$	$\geqslant 7$	7–11	8
ε_H^a ''swing''	0.18	0.14	0.12	0.17
$b_{N,0\ \text{bumpy}}^b$	0.005	0.03	−0.12	0.006
$b_{N,1\ \text{helical}}$	−0.15	−0.11	−0.2	−0.14
$b_{n,m\ \text{next}}^c$	$-0.17^{0,1}$	$-0.08^{0,1}$	$-0.15^{0,1}$	$0.02^{3N,3}$
Axis transform ι_0	0.6–1.9	0.9–2.2	0.2–0.8	1.05–1.2
Global shear (ι_a-ι_0)	−0.1→0.1	−0.07→0.17	<0.1	0.08
Magnetic wall	−1%→5%	0→6%	1.5%	0→1.6%
τ_e (ms) ISS95/expt[d]	4	9	7	4
Heating (ultimate) (ECH:RF:NBI) (MW)	0.4:0.6:0	0.6:0:3	0.5:2.5:1.5	0.2::0
Te (eV) Plan/**expt**	500/**50(Ti)**	**2,000**	**~400**[e]	1,000

[a]Helical excursion of magnetic axis normalized to major radius.
[b]Magnetic spectral component [Eq. (2)]; sign convention adjusted for consistency between devices; not normalized to aspect ratio (low aspect $\rightarrow b_{n,m}$).
[c]Next largest component and its indices n,m. For H-1, this is actually the largest term. For HSX, the component shown retains helical symmetry; the principal symmetry breaking terms are $n,m=3N,0$ and 0,2, and have smaller magnitudes, ~0.01.
[d]τ_E (planned) is dependent (via ISS95) on the assumed heating system.
[e]Spectroscopic estimate of $T_e \sim 400$ eV from initial operation with up to 350 kW ECH, 0.9 T.

II. CURRENT EXPERIMENTS

The devices reviewed (Table I) are currently operating, and have parameters in the range of major radius <1.5 m, magnetic field <1.5 T, all with relatively low aspect ratios. This creates competition between the natural toroidal components in the magnetic spectrum of low aspect ratio configurations and the helical component arising from the helical axis. The magnetic field spectrum in the straight field line, Boozer[24] coordinate system may be written as

$$B/B_0 = \sum b_{nm} \cos(n\phi - m\theta), \tag{2}$$

where n is the toroidal mode number and m is the poloidal mode number. The toroidal component $b_{0,1}$ dominates slightly in H-1, and the helical $b_{N,1}$ in TJ-II, while HSX has a virtually pure helical spectrum. This is discussed in more detail under transport.

Magnetic surfaces in this class of device tend to have markedly noncircular cross sections, and can be adjusted to be relatively free of significant islands, partly because of moderate shear inherent in helical axis configurations. The shear is generally small enough to allow very low order rational surfaces to be avoided, yet sufficient to restrict the radial extent of inevitable medium order resonances ($n,m \sim 10$). This has been confirmed by experiment in all four devices to a remarkably high precision, suggesting that vacuum magnetic surfaces in helical axis devices are particularly robust. Measured surfaces from Heliotron J,[22] traced by following low energy electron orbits, are shown in Fig. 2, and can be seen to be in good agreement with the computed surfaces (after inclusion of stray fields), confirming the accu-

racy of both the construction and modeling of the magnetic field. For the HSX configuration, behavior of magnetic surfaces for higher energy probing electrons provides an indicator of the closeness to a single helicity: the drift surfaces (traced out by particles with significant drift velocities due to their finite Larmor radius) stay close to the magnetic surfaces as shown in Fig. 3. Talmadge[23] has quantitatively confirmed the quasihelicity (also correcting for the geomagnetic field), and shown how data of this kind can be used to measure magnetic spectral components $b_{n,m}$ defined in Eq. (2).

Plasma is readily generated in TJ-II, Heliotron J, and HSX by electron cyclotron heating (ECH) at $2\omega_{ce}$. The success of second-harmonic heating shows that trapped electron losses are not serious. Initial plasma in Heliotron J achieved stored energies up to 800 J, when the resonant layer was in the range $r/a<0.8$. In H-1 rf heating is used in both nonresonant (0.05–0.2 T) and resonant modes (0.5 T) to cover a wide range of magnetic fields (Fig. 4). The convenience of the broad range of operation at low fields (over a wide range of powers ~1–100 kW) is somewhat offset by the decrease in density with magnetic field in this regime, probably due to wave penetration or propagation effects not yet fully understood. Near ion cyclotron resonance, density is recovered (and considerably improved for the light gases), but a higher power threshold is observed.

Helical axis (closed field line) configurations are highly three dimensional, and consequently require diagnostics that reflect this complexity. An example is the H-1 two-dimensional electron density interferometer shown in Fig. 5, with the data obtained. Tomographic spectroscopy and electron beam mapping systems have also been successfully employed on H-1,[25] but obtaining sufficient angular views remains an issue, in part because of the access restrictions of the configuration (principally the ring conductor).

III. TRANSPORT

Helical axis configurations benefit from an inherently high transform generated by the axis excursion, which reduces the width of banana-like orbits (especially in HSX, where quasisymmetry increases the effective transform relevant to this effect[23]). However when coupled to toroidal effects, the axis excursion tends to modulate $|B|$ to a depth of the inverse helical aspect ratio ϵ_H (≡helical axis excursion/major radius). In general this gives rise to locally trapped particles which do not benefit from drift cancellation. H-1 and TJ-II were designed to minimize the resulting toroidal mirror (or ''bumpy'') component $b_{N,0}$, but it was not possible to reduce other magnetic components as effectively, notably the toroidal curvature $b_{0,1}$ and simultaneously retain the structure of the heliac and its desirable properties, such as flexibility in transform and well. Those devices are therefore reliant on self-generated radial electric fields to achieve good confinement.

The Heliotron J configuration is designed for theoretically lower transport by inverting the sign of this ''bumpy'' component relative to the helical component. This may be thought of as placement of the trapped particle mirror bounce points in a region of magnetic field with reduced curvature.

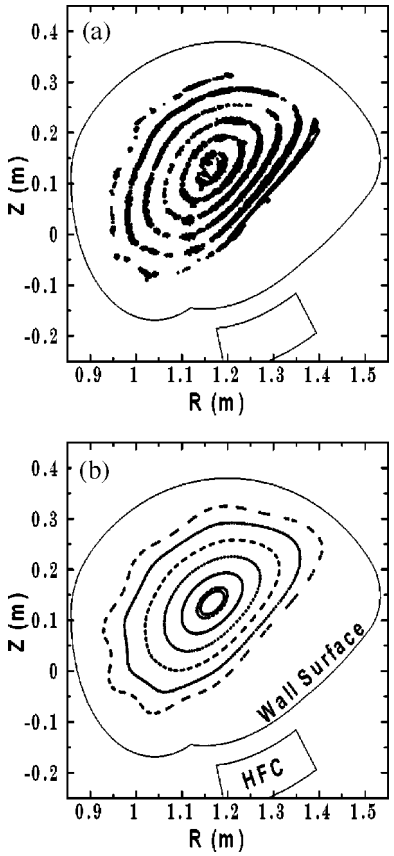

FIG. 2. Heliotron J magnetic surfaces at $\phi=67.5°$ in the standard configuration; (a) experimental results, (b) calculated (corrected for the geomagnetic field and perturbations from the local environment: HFC≡''$l=1$ helical winding'').

HSX achieves a remarkable reduction in toroidal component by a factor of 50 (computed), at the cost of a slightly higher aspect ratio, achieved by including purity of magnetic spectra as a primary design criterion. Consequently, neoclassical transport is estimated to be reduced by two orders at low collisionality, compared to a conventional stellarator with multiple periodicities in the magnetic field components. The results of initial ECH heating experiments indicate good confinement. A quantitative measure of the extent to which this

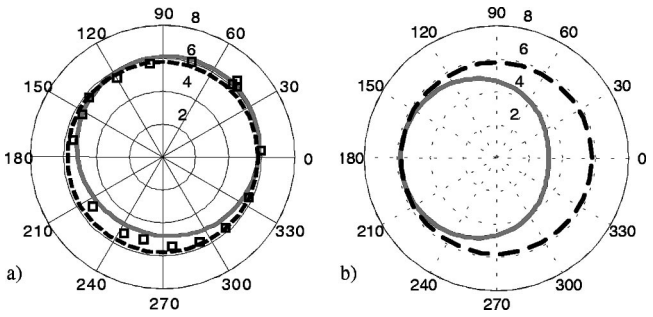

FIG. 3. HSX: (a) Measured drift orbits mapped to magnetic coordinates, ($E=450$ eV, $B\sim0.009$ T), and a curve (solid) fitted to those points in ''single-helicity'' configuration (including geomagnetic and stray fields) compared to (b) calculations for a similar configuration without helical symmetrization, illustrating reduced deviation of orbits from flux surfaces (dashed) with QHS.

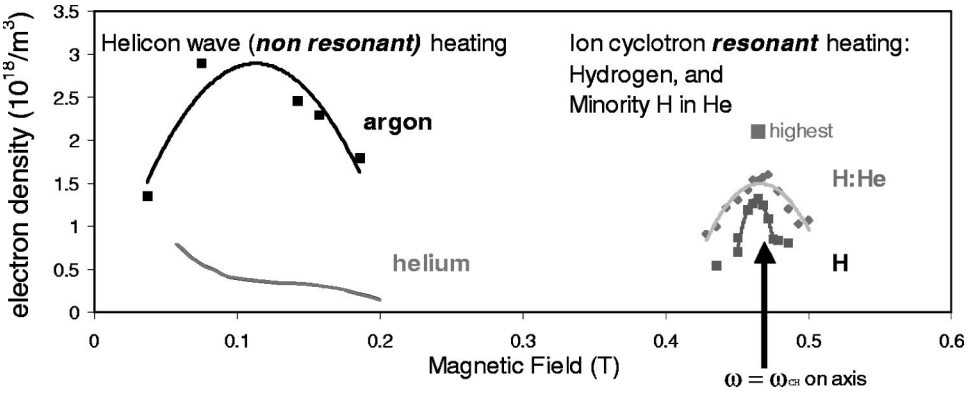

FIG. 4. H-1: Electron density for various gases at rf power 7 MHz, 60–100 kW, for both resonant ($\omega \sim \omega_{ci}$) and nonresonant ($\omega \gg \omega_{ci}$) conditions.

improvement is masked by anomalous transport will be available by comparison with the ''toroidal mirror'' configuration of HSX. This is produced by activating a subset of 48 auxiliary toroidal field coils to degrade neoclassical transport without substantially changing the plasma shape or transform.

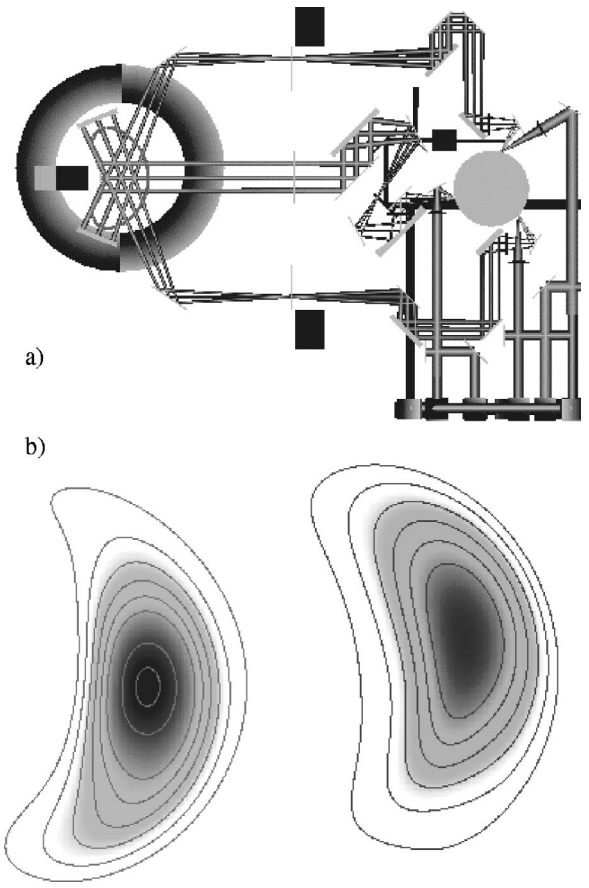

FIG. 5. a) Typical multiview diagnostic required for the high degree of nonaxisymmetry in helical axis devices. The H-1 tomographic electron density interferometer consists of a rotating wheel diffraction grating scanning three fans of 11 infrared probe beams (only 3 ×3 shown) through the bean-shaped plasma on the left. b) Time varying, 2-D reconstructed electron density profiles showing a large amplitude, global drift-like oscillation in H-1 (80 kW, 7 MHz, 0.08 T, Ar) standard configuration, at two times displaced by a $\frac{1}{4}$ period of the oscillation frequency (1.9 kHz). The reconstruction assumes a perturbation about the equilibrium flux surfaces, allows poloidal mode numbers up to $m=2$, and takes advantage of the coherence of the mode. It is not clear what relation the density contours have to magnetic surfaces at this frequency.

Experimentally, the TJ-II result[26] of $T_{e0}=2$ keV, with electron densities up to 1.2×10^{19}/m^3 and stored energies up to 1500 J, stands out as the best overall indicator of good confinement in helical axis machines to date. In a heliac, in particular, the drift orbits deviate significantly from magnetic surfaces, causing poor confinement in the absence of radial electric field.[27] That the confinement time is close to neoclassical calculations[28] including a self-consistent radial electric field (and International Stellarator Scaling:ISS95[29] scaling) indicates that such a field is counteracting orbit losses and resulting in confinement equal to other stellarators with more optimal particle orbits. Monte Carlo transport calculations used in that analysis typically show a central positive ambipolar radial electric field (100–200 V/cm: electron root) producing a potential of about +2 kV on the axis, and reasonable agreement ($\tau_E \sim 8$ ms) with experiment (5 ms). The low radiated powers (<20%) indicate that this electric field is not causing undue impurity ion accumulation, although there could be significant changes in electric field when fast ions are present, e.g., from future neutral beam injection (NBI). Further improvements may be anticipated with vacuum baking and improved ECH launching geometry. Operation of the heavy ion beam probe (HIBP) will commence shortly and provide a more complete picture of the role of potential and radial electric fields. Figure 6 shows two electron temperature profiles, one of which (with lower electron density) shows considerably more peaking inside $|r_{\text{eff}}|=3$ cm, and is suggestive of an internal transport barrier.

Configurational effects on confinement have so far been investigated mainly by varying the rotational transform in the heliacs. Degradation near low order resonances (e.g., 2/1) is observed, (e.g., TJ-II, Fig. 7) but not as markedly as in the smaller SHEILA.[30,31] When the effects of the varying volume of flux surfaces is allowed for, there is a tendency for stored energy to scale weakly with ι, qualitatively consistent with weak ι dependence (such as the ISS95 scaling of $\sim i^{0.4}$, or even iota independence). Further data and analysis including regression against power and density are required to quantify this. In the interpretation of these results, it should be remembered that there is often a peak in performance near the ''design center'' $\iota/N \sim 0.4$ (for heliacs) where many quantities are optimized, including surface quality and vol-

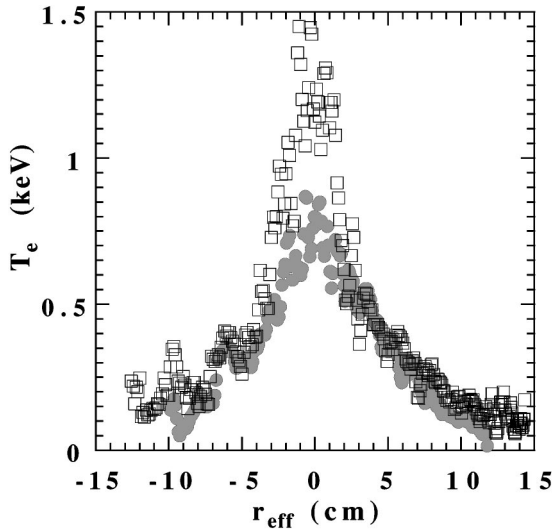

FIG. 6. TJ-II: High spatial resolution electron temperature profile in helium, 0.9 T, 300 kW, for central electron density of $\sim 0.7\times10^{19}$ m^{-3} (●) and 1×10^{19} m^{-3} (squares).

ume, and magnetic well. A qualitative weak scaling of τ_p with density and inversely with heating power is also observed.

Confinement studies on the H-1 heliac have concentrated on the plasma behavior during confinement bifurcations[32] whose features resemble low-to-high confinement transitions in bigger machines at much higher temperatures and heating powers. An example of such a transition is illustrated in Fig. 8. As the rf power is increased (in four steps) the electron density is gradually increased until at some critical power level the density suddenly increases (in less than 1 ms), while the central electron temperature (not shown) decreases by ~20%. Evolution of the plasma parameters across the transition is similar in many aspects to $L-H$ transitions in tokamaks. In particular, the transition coincides with an increase in the radial electric field and with the suppression in the fluctuation level and in fluctuation-driven particle transport. It has been shown[33] that in various scenarios it is the radial electric field that has to be driven up to a critical value for the transition to occur. The radial force balance[34]

$$E_r=(z_j e n_j)^{-1}\nabla P_j-\nu_{\theta j}B_\phi+\nu_{\phi j}B_\theta \qquad (3)$$

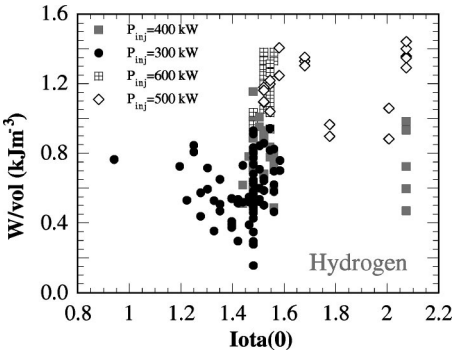

FIG. 7. TJ-II diamagnetic (stored) energy density for a range of configurations with different iota in hydrogen, normalized to plasma volume.

(where $z_j e$ is the ion charge, n_i is the ion density, P_j is the ion pressure, $\nu_{\theta i}$ and $\nu_{\phi i}$ are the poloidal and toroidal rotation velocities, respectively, and B_θ and B_ϕ are the poloidal and toroidal components of the magnetic field) has been studied experimentally using various probes.[35]

A key feature of these H-1 plasmas is the absence of bulk rotation; it has been found both by probe and spectroscopic studies that the mass flow velocities are much less ($<1/10$) than the **E×B** drift velocity, so that the radial electric field in Eq. (3) is balanced on average by the ion pressure gradient. This is illustrated in Fig. 8(b), where poloidal velocity is shown to be much smaller than **E×B**. This effect, namely, a small role of the mass flow in the radial force balance ($E_r=\nabla p_i/(Zen_e)$) has also been confirmed dynamically during spontaneous transitions from low to high confinement as shown in Fig. 8(b) (inset). Since the ion saturation current there is proportional to $I_s\sim n_e\sqrt{T_e+T_i}$, we use it as an approximate measure of the ion pressure, since $T_i > T_e$ in argon plasma in H-1. The approximate values of ∇p and E_r track quite closely in time. An important conclusion[33] is that it is the sheared electric field (or sheared **E×B** drift) that affects the fluctuations and the fluctuation-driven transport. In other words, it is the sheared potential flows that modify the fluctuations and transport in H-1. In the TJ-II heliac, strong shear in E_r is observed across rational surfaces [e.g., $(dE_r/dr)/B\sim10^5$ s^{-1} across the $n/m=8/5$ surface]. This is interpreted[36] as high shear in the **E×B** flow, and (its inverse) is comparable with the fluctuation decorrelation time.

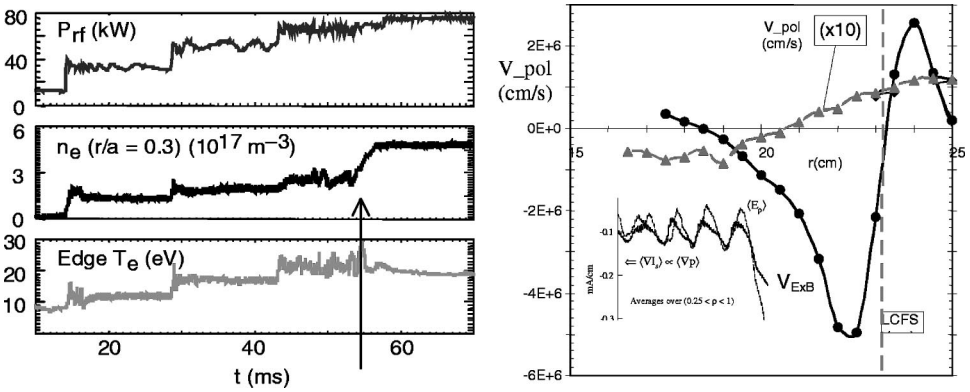

FIG. 8. (a) A confinement transition in H-1 showing applied heating power, electron density near the axis, and edge electron temperature. The arrow shows the transition to improved confinement. (b) Radial profile comparing poloidal bulk velocity (magnified ×10) with **E×B**. (Argon plasma, $n_{e0}=2\times10^{18}$, $B=0.07$ T, $\iota\sim1.45$.) Inset: Time evolution of the average radial gradient of the ion saturation current solid line and the average radial electric field (dashed line) for a $L\rightarrow H$ transition.

The interaction between fluctuation and flow has been studied experimentally in H-1. It has been found that depending on the shape of the radial electric field profile, strong sheared E_r can either suppress turbulence (when $E_r' < 0$, where the prime here indicates d/dr), or change the phase difference between potential and density fluctuations leading to a reduction or even to a radial reversal of the fluctuation-produced transport (when $E_r' > 0$).[37] The latter effect (Γ_{fl} reversal correlated with $E_r' < 0$) has been also confirmed in the CHS heliotron/torsatron[38] where the formation of the $E_r' < 0$ region in the plasma edge using edge ECH has led to a local reversal of Γ_{fl}. It is possible that the observed inward transport can explain inward convection observed in other tokamak and stellarator experiments (for example, in W-7AS[39]).

IV. STABILITY

The simplest stability criterion, the existence of a magnetic well [Eq. (1)], was a primary motivation behind the inception of the heliac,[6] and is also present in Heliotron J and HSX. Further, the flexibility of these devices allows the magnetic well to be greatly reduced, and to some extent, inverted into at least a partial magnetic hill. The question[40] of whether local V'' is more or less important than the total change in V' is relevant, as all these machines have a number of configurations that exhibit a region of positive V'' near the last closed surface. Ballooning instabilities must be considered, as the minimum average B is achieved by connecting regions of good and bad curvature. In general, the helical axis generates rather large rotational transform, which keeps the connection length short, typically one field period. Estimates of critical β_c for ballooning vary from 0.6% to 2% across various configurations of each machine, and using various methods,[41] the lower values being of interest in the hope that ballooning instabilities may be experimentally accessible in some configurations of the existing devices with limited plasma heating power. Critical β values for Mercier stability are found to be typically a little higher than for ballooning in heliacs, and a little lower in HSX. Quasihelical configurations capable of $\beta_c \sim 10\%$ (ballooning) have been found.[42]

It is therefore not surprising that results to date (at low β) have indicated good stability, and in common with other ''current free'' stellarators, the absence of plasma disruptions. Coherent drift-like modes have been observed in SHEILA, where a relation to rotational transform and mode number was found.[30] The physical description and analysis was greatly simplified by the use of (approximate) magnetic coordinates. A similar mode is also seen in H-1 at very low fields (<0.15 T), but a clear connection with local curvature or magnetic well has not been found so far. Persson *et al.*[43] have recently treated drift modes in full helical stellarator geometry.

Such strong fluctuations are typical (but not necessary) for ''*L*-mode'' plasmas in H-1. A composite triple-probe/radial Mach-probe/triple probe (TMT probe) and an associated iterative technique have been developed which allow measurements of probe potentials and saturation currents to be combined to produce computed signals for the *fluctuating* density and electron and ion temperatures. In the first instance, this analysis assumes the fluctuation-induced particle flux is ambipolar. Application of this technique to sample *L*-mode discharges yields derived signals with $\tilde{n}/n \approx \tilde{T}_e/T_e \approx 30\%$.

In TJ-II, density fluctuations of 10%–40% are seen near the edge, for frequencies up to 200 kHz. Furthermore, fluctuation levels and the radial electric field at the plasma edge have been observed to vary between several similar configurations in which the main distinguishing feature was the magnetic well depth,[44] reduced amplitude being associated with deeper well. Further progress in the relationship between stability and magnetic well (and shear and transform) can be expected in the near future, as improvements in power supply control allow very precise matching of other characteristics of the magnetic configuration as the well is varied. Edge localized mode (ELM)-like MHD events observed in the Mirnov coils in TJ-II, for stored energies near 1 kJ appear to be associated with changes in transport localized at $\langle r \rangle / \langle a \rangle \sim 0.6$. This is in a region of high pressure gradient, and may be indicative of resistive ballooning instabilities.[26] Neutral beam injection in TJ-II (2001) and Heliotron J(FY2000-2) should provide access to sufficiently high $\beta > 1\%$ to probe this important physics regime more thoroughly.

V. SUMMARY AND DISCUSSION

The results from the experiments reported here are very encouraging. In all cases, magnetic surfaces were of high quality in the configurations as built, and plasma formation was straightforward. At this stage, there are no requirements for compensation of magnetic field errors, although all groups are actively monitoring magnetic fields and possible errors and means for introducing and/or correcting them. Confinement results are equally encouraging, particularly since all experiments to date use second-harmonic heating, which should accentuate orbit problems with high perpendicular electron energy. Raw data from several machines imply confinement times > 2–3 ms, close to ISS95 scaling, and full transport analysis including estimates of absorbed power and profile data will only improve those results. The most mature ECH results are those of TJ-II with 2 keV electron temperature, 1500 J stored energy, and $\sim > 5$ ms confinement times, comparable to the best stellarator results of machines this size, and indicating implicitly the successful formation of self-consistent radial electron root electric fields required for orbit loss reduction. This is a central issue in stellarator physics, and future HIBP data should provide direct evidence of this phenomenon. The direct comparison of results from very similar configurations but with very different predictions of neoclassical transport possible in HSX will be a very significant experiment. Confinement transitions demonstrated at low powers in H-1 provide much insight into basic physics, and future experiments will expand this data by investigation of the influence of electric fields imposed by localized ECH. Impurity accumulation has not been serious in

operations to date, consistent with the polarity of the inferred radial field. Ion heating data from NBI injection and ICRH will be the key test of this phenomenon.

No dangerous instabilities have been observed, but the flexibility of all devices will allow probing of stability limits. Ballooning stability is a key issue, and predictions show that experiments with NBI capability, TJ-II, and Heliotron J, should have access to sufficiently high $\beta > 1\%$ to access this physics regime. In the near term, all devices can seek degraded stability regimes for physics studies by virtue of their flexibility. The ease of operation at second-harmonic ECH shows that investigation of trapped electron instabilities, although so far not identified, should be possible.

The four machines described form a set of similar devices with some very interesting differences in characteristics and capabilities. Data to date are very encouraging, and generally show consistency between the devices. As the machines mature, the various special features are developed, and data becomes more refined, detailed contrast and comparisons will be possible. A significant challenge is to make best use of the extreme flexibility of these devices to elucidate the basic physical processes. The potential exists to clearly separate fundamental but normally inter-related issues of resonances in transform, magnetic shear and magnetic curvature.

ACKNOWLEDGMENTS

The author gratefully acknowledges all members of the TJ-II, Heliotron J, HSX, and H-1 groups for their contributions and access to their data, in particular C. Alejaldre, E. Ascasibar, C. Hidalgo, T. Obiki, K. Nagasaki, D. T. Anderson, J. N. Talmadge, F. S. Anderson, J. H. Harris, M. G. Shats, J. Howard, N. Gyaltsin, S. M. Collis, and D. L. Rudakov.

[1] L. Spitzer, Jr., Phys. Fluids **1**, 253 (1958).
[2] A. I. Morozov and L. S. Solov'ev, in *Reviews of Plasma Physics*, edited by M. A. Leontovitch (Consultants Bureau, New York, 1966), Vol. 2, p. 1.
[3] H. R. Koenig, U.S. Atomic Energy Commission Report No. NYO-7310 (PM-S-20), 1956.
[4] J. L. Johnson, C. R. Oberman, R. M. Kulsrud, and E. A. Frieman, Phys. Fluids **1**, 281 (1958).
[5] H. P. Furth, J. Killeen, and M. N. Rosenbluth, Phys. Fluids **6**, 459 (1963).
[6] H. P. Furth, J. Killeen, M. N. Rosenbluth, and B. Coppi, in *Plasma Physics Controlled Nuclear Fusion Research*, Proceedings of the Second International Conference, Culham, 1965 (International Atomic Energy Agency, Vienna, 1966), Vol. 1, p. 103.
[7] W. D. D'haeseleer, W. N. G. Hitchon, J. Callen, and J. L Shohet, *Flux Coordinates and Magnetic Field Structure* (Springer, Berlin, 1990).
[8] H. P. Furth, in *Advances in Plasma Physics*, edited by A. Simon and W. B. Thompson (Wiley Interscience, New York, 1967), Vol. 1, p.76.
[9] J. Greene, Comments Plasma Phys. Control. Fusion **17**, 389 (1997).
[10] S. Nagao, H. Watanabe, Y. Funato *et al.*, *Proceedings of the Seventh Symposium on Engineering Problems of Fusion Research, Knoxville, TN* (IEEE, New York, 1977), Vol. 1, pp. 841–845.
[11] S. Yoshikawa, *Proceedings of the Fourth International Stellarator Workshop, Cape May, NJ* (International Atomic Energy Agency, Vienna, 1982), Vol. 2, pp. 1–22.
[12] A. H. Boozer, T. K. Chu, R. L. Dewar *et al.*, in *Plasma Physics Controlled Nuclear Fusion Research* (International Atomic Energy Agency, Vienna, 1983), Vol. III, p. 129.
[13] S. Yoshikawa, Nucl. Fusion **23**, 667 (1984).
[14] B. D. Blackwell, S. M. Hamberger, L. E. Sharp, and X. H. Shi, Nucl. Fusion **25**, 1485 (1985).
[15] S. Kitajima, M. Takayama, T. Zama *et al.*, Jpn. J. Appl. Phys., Part 1 **27**, 2606 (1991).
[16] S. M. Hamberger, B. D. Blackwell, L. E. Sharp, and D. B. Shenton, Fusion Technol. **17**, 123 (1990).
[17] C. Alejaldre, J. J. Alonso, J. Botija *et al.*, Fusion Technol. **17**, 131 (1990).
[18] C. M. Greenfield, M. E. Koepke, and F. L. Ribe, Phys. Fluids B **2**, 133 (1990).
[19] F. Bauer, O. Betancourt, and P. Garabedian, *Magnetohydrodynamic Equilibrium and Stability of Stellarators* (Springer, Berlin, 1984); P. R. Garabedian and H. J. Gardner, in *Computational Techniques and Applications: CTAC 95, Proceedings of the Seventh Biennial Conference, July 1995*, edited by R. L. May and A. K. Easton (World Scientific, Singapore, 1996).
[20] D. A. Monticello, R. L. Dewar, H. P. Forth, and A. Reiman, Phys. Fluids **27**, 1248 (1984).
[21] J. H. Harris, J. L. Cantrell, T. C. Hender, B. A. Carreras, and R. N. Morris, Nucl. Fusion **25**, 623 (1985).
[22] T. Obiki, T. Mizuuchi, K. Nagasaki *et al.*, ''First plasmas in Heliotron J,'' Plasma Physics Controlled Nuclear Fusion Research, Proceedings of the 18th Fusion Energy Conference, Sorrento 2000 (International Atomic Energy Agency, Vienna), IAEA-CN-77/EXP1/09, to be published.
[23] J. N. Talmadge, V. Sakaguchi, F. S. B. Anderson *et al.*, ''Drift orbit and magnetic surface measurements in the helically symmetric experiment,'' in Ref. 22, IAEA-CN-77/EXP1/06, to be published.
[24] A. H. Boozer, Phys. Fluids **23**, 904 (1980).
[25] J. Howard, B. D. Blackwell, G. G. Borg *et al.*, J. Plasma Fusion Res. **1**, 342 (1998); J. Howard, Rev. Sci. Instum. (to be published).
[26] C. Alejaldre, J. Alonso, L. Almoguera *et al.*, ''Review of confinement and transport studies in the TJ-II flexible heliac, '' in Ref. 22, IAEA-CN-77/OV4/4, to be published, and references therein.
[27] E. R. Solano, J. A. Rome, and S. P. Hirshman, Nucl. Fusion **28**, 157 (1988); S. A. Dettrick, S. S. Lloyd, H. J. Gardner, R. L. Dewar, and S. L. Painter, *ibid.* **38**, 1001 (1998).
[28] V. Tribaldos and B. Ph. Van Milligen, Nucl. Fusion **36**, 283 (1996); F. Castejón, V. Tribaldos, I. García-Cortés *et al.*, ''Enhanced heat confinement in TJ-II,'' submitted to Nucl. Fusion.
[29] U. Stroth, M. Murakami, R. A. Dory *et al.*, Nucl. Fusion **36**, 1063 (1996).
[30] X.-H. Shi, S. M. Hamberger, and B. D. Blackwell, Nucl. Fusion **28**, 859 (1988).
[31] X.-H. Shi, B. D. Blackwell, and S. M. Hamberger, Plasma Phys. Controlled Fusion **31**, 13 (1989).
[32] M. G. Shats, D. L. Rudakov, B. D. Blackwell *et al.*, Phys. Rev. Lett. **77**, 4190 (1996).
[33] M. G. Shats, C. A. Michael, D. L. Rudakov, and B. D. Blackwell, Phys. Plasmas **5**, 2390 (1998).
[34] J. N. Talmadge and M. G. Shats, ''Radial force balance in stellarators,'' submitted to Phys. Plasma.
[35] M. G. Shats, D. L. Rudakov, R. W. Boswell, and G. G. Borg, Phys. Plasmas **4**, 3629 (1997); D. L. Rudakov, M. G. Shats, J. H. Harris, and B. D. Blackwell, ''Dynamic behavior of the low to high confinement transitions in the H-1 heliac,'' to appear in Plasma Phys. Controlled Fusion.
[36] C. Hidalgo, M. A. Pedrosa, E. Sanchez *et al.*, Plasma Phys. Controlled Fusion **42**, A153 (2000).
[37] M. G. Shats and D. L. Rudakov, Phys. Rev. Lett. **79**, 2690 (1997); M. G. Shats, Plasma Phys. Controlled Fusion **41**, 1357 (1999).
[38] M. G. Shats, K. Toi, K. Ohkuni *et al.*, Phys. Rev. Lett. **84**, 6042 (2000).
[39] U. Stroth, T. Geist, J. P. T. Koponen *et al.*, Phys. Rev. Lett. **82**, 928 (1999).
[40] B. McNamara, K. J. Whiteman, and J. B. Taylor, in *Plasma Physics Controlled Nuclear Fusion Research*, Proceedings of the Second International Conference, Culham, 1965 (International Atomic Energy Agency, Vienna, 1983), Vol. I, p. 145.
[41] H. J. Gardner and B. D. Blackwell, Nucl. Fusion **32**, 2009 (1992); J. N. Talmadge and W. A. Cooper, Phys. Plasmas **3**, 3713 (1996).
[42] J. Nuhrenberg and R. Zille, Phys. Lett. A **29**, 113 (1988).
[43] M. Persson, M. Nadeem, J. L. V. Lewandowski, and H. J. Gardner, Plasma Phys. Controlled Fusion **42**, 203 (2000).
[44] J. Castellano, J. A. Jiménez, C. Hidalgo *et al.*, ''Magnetic well and instability thresholds in the TJ-II stellarator,'' submitted to Nucl. Fusion.